RESEARCH ARTICLE | FEBRUARY 10 2023

Influence of oxygen on the optical, electrical, and heating properties of gallium-doped zinc oxide (GZO) films

Jasmine Beckford ; Makhes K. Behera ; Kelsea Yarbrough ; Sangram K. Pradhan ; Messaoud Bahoura

AIP Advances 13, 025249 (2023)
https://doi.org/10.1063/5.0134151
CHORUS

Influence of oxygen on the optical, electrical, and heating properties of gallium-doped zinc oxide (GZO) films

Cite as: AIP Advances 13, 025249 (2023); doi: 10.1063/5.0134151
Submitted: 11 November 2022 • Accepted: 26 January 2023 •
Published Online: 10 February 2023

Jasmine Beckford,[1,a] Makhes K. Behera,[1] Kelsea Yarbrough,[1] Sangram K. Pradhan,[1,b] and Messaoud Bahoura[1,2]

AFFILIATIONS

[1] Center for Materials Research, Norfolk State University, 700 Park Avenue, Norfolk, Virginia 23504, USA
[2] Engineering Department, Norfolk State University, 700 Park Avenue, Norfolk, Virginia 23504, USA

[a] Electronic mail: j.z.beckford@spartans.nsu.edu
[b] Author to whom correspondence should be addressed: skpradhan@nsu.edu

ABSTRACT

Thin-film transparent heaters (TFTHs) are gaining popularity in optoelectronics and a variety of domestic applications, including smart windows, car defrosters, and other devices. The deposition and characterization of TFTHs made of gallium-doped zinc oxide (GZO) are presented in this work. GZO thin films were deposited via pulsed laser deposition on glass substrates with varying oxygen partial pressures from 0 to 10 mTorr during deposition. The samples demonstrated very low sheet resistance values between 5 and 17 Ω/sq from 0 to 10 mTorr, respectively. UV/vis transmission spectra revealed that TFTHs have a high optical transparency above 80%. GZO-based TFTHs demonstrated a consistent and repeatable joule heating effect, with temperatures reaching 76 °C with a low input voltage of 10 V. This research could guide the future use of GZO as a transparent conducting oxide material for many potential cost-effective applications from low-powered electronics to lightweight and wearable devices.

INTRODUCTION

Transparent conducting oxide (TCO) materials are materials that possess sheet resistance values of 1–250 Ω/sq and optical transmittance >85% in the visible wavelength region.[1–4] Currently, indium-doped tin oxide (ITO), the commercially used TCO, is facing more difficulties due to the high cost and scarcity of indium. Indium, which is produced as a by-product of Zn, Cu, and Sn ores, is a depleting resource resulting in a rapidly increasing price, making it a lower performance-to-cost ratio option. Furthermore, ITO films are also brittle, making them unsuitable for long-run bendable/foldable electronic devices. Therefore, considering the wide range of applications requiring a flexible electrode, ITO fails to satisfy such requirements.[5–8]

Numerous alternatives have been studied to find a replacement for ITO for a variety of high-performance optoelectronic applications. Some examples include graphene, networks of carbon nanotubes in the form of 2D films, and conductive percolation networks with optimum transparency. In particular, these materials demonstrated joule heating effects upon application of voltage, which allows for them to possess the qualities of a transparent heater. These qualities of a transparent heater can be used for a wide range of applications, such as defrosting in mirrors and windows, outdoor displays, smart windows, de-icing, and heaters in wearable devices.[9–12]

Metal nanostructures, especially silver nanowires/mesh, are among the most promising alternatives to ITO due to their excellent electrical conductivity, mechanical stability, and high optical transmittance in the visible wavelength region for thin-film heaters (TFHs).[13–17] However, these silver-based nanowires suffer from dissatisfactory interconnections between the random networks and a high junction resistance.[18–22] These disadvantages affect the electrical and heating properties of the thin film. Other effective alternatives are graphene and carbon nanotubes.[23–25] They offer a

high optical transparency and an excellent electrical and thermal conductivity.[26,27] However, carbon nanotubes and graphene tend to be expensive during the fabrication process, which restricts their widespread use in practical applications.[28,29]

Metal oxide-based TCOs, such as doped ZnO films, exhibit an excellent electrical conductivity and a high optical transparency and can overcome the previously stated difficulties better than the above-mentioned materials. By substituting part of the Zn atoms with higher valence elements, such as Al and Ga, the electrical characteristics of ZnO films can be greatly improved.[30–36] Gallium and aluminum are the best dopants for maintaining the transparency and conductivity of the ZnO film. The smaller ionic radius of the Ga and Al atoms with respect to the Zn atoms allows them for an effective substitution at the Zn site of the ZnO matrix during doping. The close atomic size of Ga and Al, which are used as a substitute element, also helps to prevent any kind of substantial structural deformation in the unit cell. The addition of oxygen during deposition has been proposed to tune the transparency and conductivity of Ga-doped ZnO (GZO) thin films grown by the ion-plating method.[37]

In this article, we investigate the effect of oxygen partial pressure during thin film deposition on an effective, low-powered GZO thin film grown by pulsed laser deposition (PLD) for transparent heater applications. The films demonstrated low sheet resistance values (5 and 17 Ω/sq) and a high optical transmittance (>80%), which encourage the use of the GZO material as a thin-film heater for different applications, such as automobile defrosters, LED displays, and smart windows.

EXPERIMENT

Preparation of GZO target with the composition $Ga_{0.07}Zn_{0.93}O$

High purity (99.99%) Ga_2O_3 and ZnO powders are used as raw materials to prepare the Ga doped ZnO target in the composition of $Ga_{0.07}Zn_{0.93}O$ through a solid state route. In the first step, stoichiometric amounts of Ga_2O_3 and ZnO powders are taken and thoroughly mixed for several minutes at room temperature using a mortar and pestle. The powder mixture is poured into a high temperature alumina crucible and placed inside the furnace at the temperature of 800 °C. Every 4 h, the powder mixture was quenched and grinded until it breaks into an ultrafine form. Ultimately, the fine powder of the Ga doped ZnO is pressed into a 1-in. dia punch via a hydraulic press to make the final target. The prepared target went into the final step of sintering at 1200 °C for 12 h in air to obtain a compact structure.

Deposition of GZO thin films

The above prepared GZO target was loaded into the PLD chamber (Neocera make). GZO thin films are deposited at very high vacuum with the base pressure of chamber in the order of 10^{-8} Torr. Before placing the substrates into the PLD chamber, the glass substrates used for depositing the films were thoroughly cleaned sequentially with acetone, methanol, and de-ionized (DI) water and dried by flowing N_2 gas. The GZO thin films were deposited on glass substrates with the oxygen partial pressure ranging from 0 to 10 mTorr and at the substrate temperature of 350 °C. During deposition, the excimer laser energy used for this growth was varied between 200 and 250 mJ per unit area with a repetition rate of 7 Hz and the distance between the substrate and target was maintained at 5 cm. Various numbers of laser pulses were used to achieve the optimum thickness of the GZO thin film for our study.

Characterization of GZO thin films

The structural, electrical, optical, and electro-thermal properties of the GZO thin films were investigated using a variety of methods. The crystal structure of the films was examined using a Panalytical X'Pert Pro high-resolution x-ray diffractometer using Cu K_α radiation. The temperature dependent resistivity properties of the films were measured using a linear four-probe employing a Keithley nanovoltmeter and a current source connected to a PC using LabVIEW software. A Perkin Elmer Lambda 950 UV/vis spectrometer was used to study the optical characteristics of the films grown under various conditions. The electro-thermal properties (heating effect of the GZO based TFTH) of the GZO thin films were determined using an external DC voltage source, and the temperature of the films is recorded with the help of an ultrasensitive FLIR thermal camera. X-ray photoelectron spectroscopy (XPS) of the samples was performed to verify the oxidation states and analyze the composition of the GZO thin films.

RESULTS AND DISCUSSION

Structural properties

The x-ray diffraction (XRD) data of the GZO thin films deposited on silicon substrates show the presence of a diffraction peak at ~34.56°, slightly higher than the standard ZnO powder diffraction angle of 34.45° (Fig. 1). The results show the possibility of the development of tensile stress in the plane of the film by the substrate. This effect may be attributed to the doping of Ga into ZnO as the radius of Zn is greater than that of Ga. As Ga exchanges the element on the Zn site, the lattice parameter decreases along the c-axis and increases the diffraction angle.

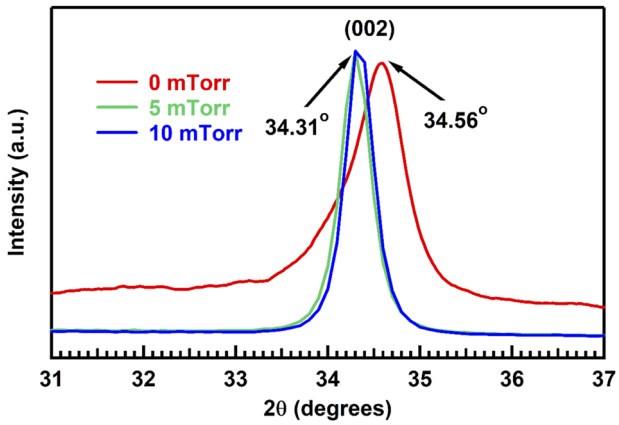

FIG. 1. X-ray diffraction patterns of GZO thin films at different oxygen partial pressures.

The results indicate that all films are polycrystalline and show a preferential orientation in the (002) direction exhibiting the c-axis perpendicular to the substrate. The presence of a (002) plane of GZO and the intense peak at a 2θ angle of ~34.56° confirms the presence of GZO. The XRD data shift to lower diffraction angles with the increase in the oxygen pressure during deposition. The contribution of oxygen identifies a decrease in oxygen vacancies present.[38–42] A decrease in the oxygen vacancy results in a decrease in the out-of-plane lattice parameter, thus moving the lattice closer to the bulk value, as shown in previous studies on oxides and perovskite structures.[43–45] Figure 1 is normalized to provide more distinguished shifted peaks in relation to the oxygen pressure. Using the Scherrer equation,[46,47] the calculated crystallite sizes of the films ranged from 10.7 to 21.3 nm when the oxygen partial pressure increased from 0 to 10 mTorr (Table I). The increase in the oxygen partial pressure narrows the full width at half maximum (FWHM) of the (002) peak, which shows an increase in the crystallite size of the film.

Optical properties

Figure 2 displays the optical transmittance spectra of the GZO films deposited on glass substrates measured in air at room temperature as a function of different oxygen partial pressures. The optical transmission data shown in the figure exhibit an excellent transparency in the visible wavelength region with an observed average percentage transmission of over 80% and a sharp fall in the transmittance at the absorption edge at ~330 nm. The optical transmission of the GZO films is slightly improved by increasing the oxygen partial pressure (10 mTorr).

The Tauc plot has been used to determine the optical energy bandgap of GZO thin film grown at different oxygen partial pressures, as shown in Fig. 3. The bandgap of GZO thin films at 0 mTorr oxygen partial pressure is ~3.48 eV, which is a little bit higher than the bulk ZnO, which may be due to the quantum confinement in nanocrystalline GZO.[48] Using a linear fitting of the data close to the absorption edge from the Tauc plot, $(\alpha h\nu)^2 = A(h\nu - E_g)$,[49–52] at oxygen partial pressures of 5 and 10 mTorr, the calculated bandgaps are 3.32 and 3.44 eV, respectively. The reduction in the bandgap could be attributed to a decrease in the charge carrier concentration caused by the filling up of the oxygen vacancy sites as the oxygen partial pressure is increased during deposition. This leads to electron–electron collisions and agrees with the results of electrical properties discussed later.[53]

Composition analysis

The XPS characterization is performed on the samples grown at varying oxygen partial pressures (0–10 mTorr). The XPS background was subtracted, and a Gaussian-shaped profile was used to find the fitting peak for the high-resolution XPS spectra analysis. Figure 4 displays the oxygen peaks present in the samples between 525 and 535 eV. The fitted peaks were split into three separate peaks (lattice, vacancy, and adsorbed) to determine the ratio of the metal-bonded oxygen to the oxygen vacancies.[54,55] This ratio is calculated by determining the area under each of the peaks and taking their ratio.[56] The $O_{vacancy}/O_{lattice}$ ratios for the films grown under the oxygen partial pressures of 0, 5, and 10 mTorr are found to be 0.94, 0.74, and 0.70, respectively. As expected, with an increase in the oxygen partial pressure during deposition, the ratio $O_{vacancy}/O_{lattice}$ was found to decrease, indicating an increase in the oxygen concentration in the films.

TABLE I. Variation of the 2θ peak, full width at half maximum (FWHM), grain size (D), and optical bandgap (E_g) with the oxygen partial pressure (PO_2).

Oxygen partial pressure (PO_2)	0 (mTorr)	5 (mTorr)	10 (mTorr)
2θ (°)	34.56	34.31	34.31
FWHM (°)	0.78	0.40	0.39
D (nm)	10.67	20.79	21.32
E_g (eV)	3.48	3.32	3.44

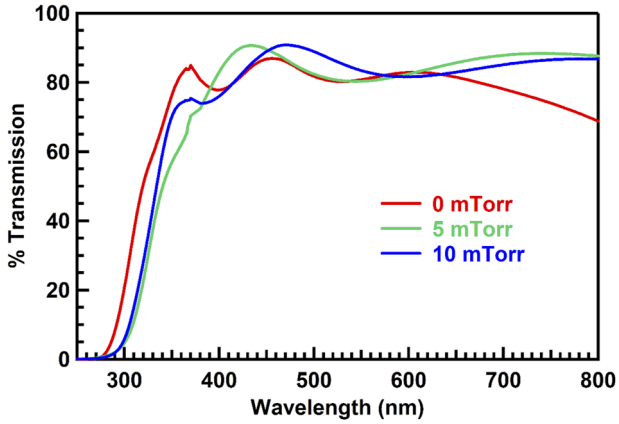

FIG. 2. Optical transmittance spectra of GZO thin films as a function of oxygen partial pressure.

Electrical properties

The GZO films are grown on glass substrates to determine the electrical properties of the films. Temperature-dependent measurements are performed using the linear four-probe technique, and the

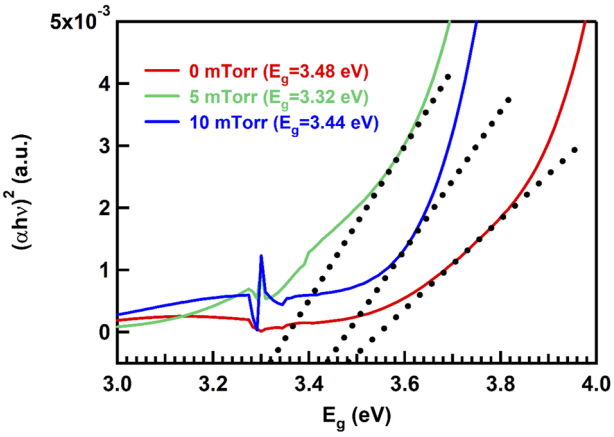

FIG. 3. Tauc's plot of GZO films grown under different oxygen partial pressures.

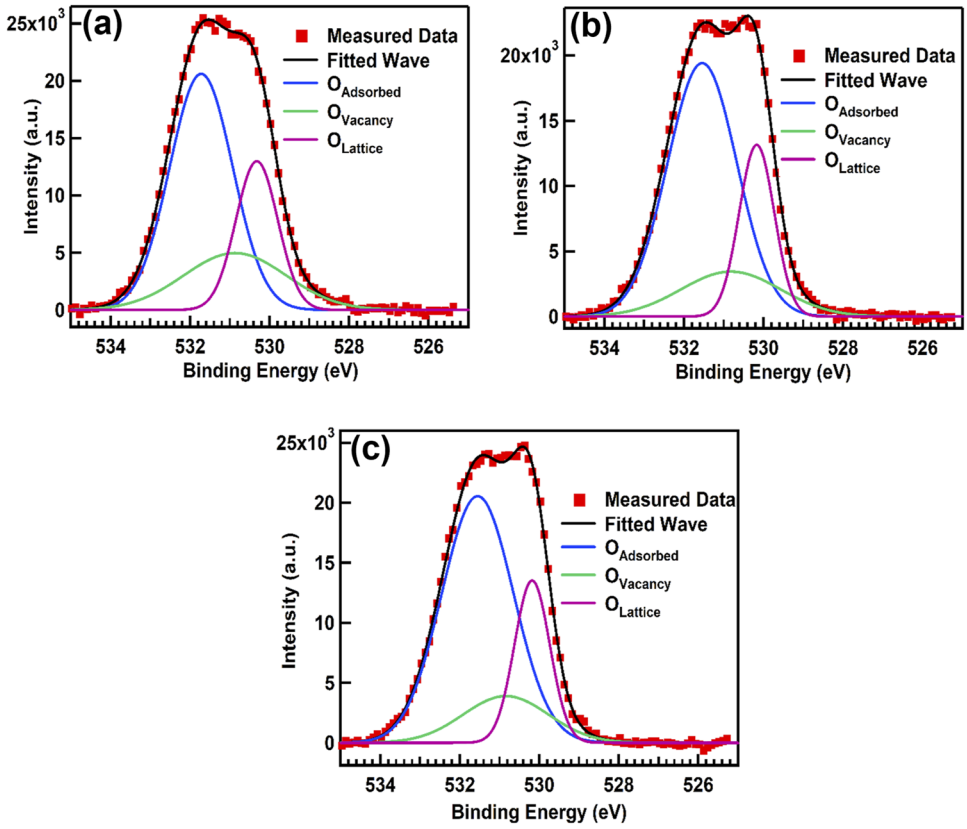

FIG. 4. XPS graphs of GZO thin films at different oxygen partial pressures: (a) 0 mTorr, (b) 5 mTorr, and (c) 10 mTorr.

results are shown in Fig. 5. ZnO is a very well-known wide bandgap material semiconductor and shows a considerably higher resistivity and exhibits a semiconducting behavior. In this study, the doping percentage of Ga in the ZnO matrix of the deposited films is 7% and the composition of the sample is $Ga_{0.07}Zn_{0.93}O$. The varying oxygen partial pressure had an inverse effect on the GZO thin film electrical conductivity due to the decrease in oxygen vacancies. The sample grown at 0 mTorr oxygen partial pressure shows the formation of vacancies, and the oxygen vacancies increase the carrier concentration considerably. The observation of metallic characteristic and lower resistivity of ZnO thin films is a combined effect of Ga doping and oxygen vacancies, which act as donors and lead to degeneracy. The temperature dependent resistivity from room temperature to a higher temperature (90 °C) of this film shows a positive temperature coefficient of resistivity (TCR) as the resistance of the sample increases with increasing temperature as shown in Fig. 5(a). Hence, the observation of the metallic type characteristic in resistivity–temperature measurement can be explained by the formation of a degenerate band appearing in the sample, where the Ga atoms are heavily doped in the ZnO semiconductor film as well explained by Mott *et al.*[57] Similarly, positive TCR characteristics are noticed and have also been reported by other research groups through studying metal doped ZnO and other semiconducting material systems.[58–61] Furthermore, 5 mTorr samples also show the same behavior of the temperature dependent resistive curve as shown in Fig. 5(b). This agrees with the trend seen in the calculation of the bandgap of the films, which is found to decrease as the charge carrier concentration increases. Furthermore, the oxygen vacancy concentration decreased in the sample grown at 10 mTorr oxygen partial pressure and favored a plunge in the number of oxygen vacancies. The decrease in the carrier concentration of oxygen vacancies also shifts the Fermi level below the conduction band and, thus, explains the observed semiconducting behavior in the resistivity–temperature curve by slightly decreasing the resistivity with increasing the temperature as shown in Fig. 5(c).

Electro-thermal properties

After validating that the GZO thin films are transparent and conductive, the electro-thermal properties of the films are studied to test their application as TFTHs. The GZO thin films are supplied with an external DC voltage, and the generated heat is monitored (Fig. 6).

Using a FLIR camera, we recorded the thermal images of the samples (Fig. 7). The FLIR images show a uniform heat distribution between the electrodes and the highest heat at the center of the thin films. All films are conductive and generate heat at different applied voltages ranging from 0 to 10 V. The sample grown at 10 mTorr partial oxygen pressure shows the highest temperature of up to 76 °C, which could be due to the higher resistive nature. The oxygen vacancy is normally formed in GZO samples that are

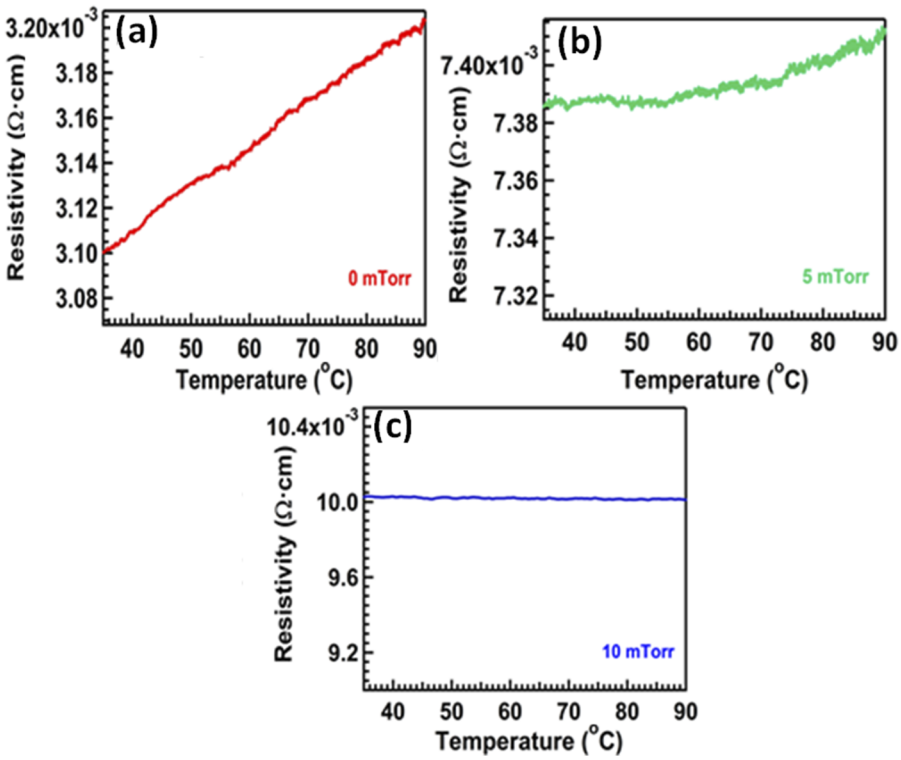

FIG. 5. Measurement of electrical properties (resistivity vs temperature) of GZO thin films grown at different oxygen partial pressures using the linear four-probe technique: (a) 0 mTorr, (b) 5 mTorr, and (c) 10 mTorr.

grown in a higher vacuum environment. However, a higher oxygen partial pressure favors the reduction in oxygen vacancies as observed in our 10 mTorr sample and also as confirmed through the XPS study as well. This film can generate nearly 76 °C of heat at a DC voltage of only 10 V. This is a remarkable property that can be used in various thin-film heating applications. We list the several experimental research findings obtained by other researchers about the GZO, AZO (Al-doped ZnO film), FTO (fluorine-doped

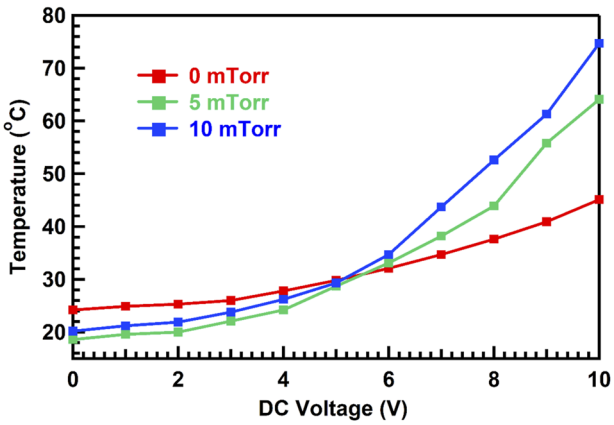

FIG. 6. Electro-thermal measurements of the GZO thin films grown on glass substrates at different partial oxygen pressures using a DC power supply.

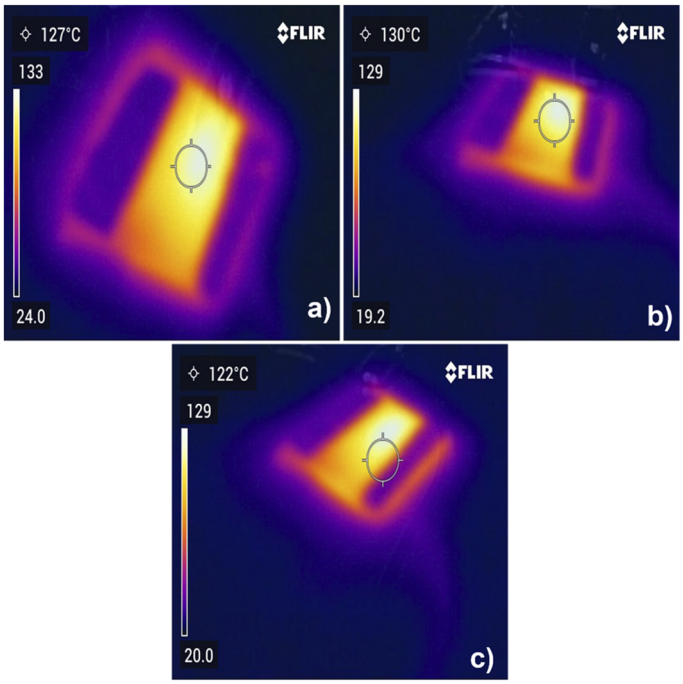

FIG. 7. Joule heating effect displayed by the GZO thin films at different oxygen partial pressures of (a) 0 mTorr, (b) 5 mTorr, and (c) 10 mTorr, captured using a FLIR camera.

TABLE II. Comparison study of different TCO thin films, such as AZO, GZO, fluorine-doped tin oxide (FTO), and AZO/FTO double layer thin films, through resistivity, substrate temperature (T_s), optical transmission, thin film growth technique, applied voltage to measured heating effect in temperature (°C) of the current work (last row) with other reported studies.

Resistivity	T_s (°C)	Transmission (%)	Deposition method	Applied volt. (V)	Temperature (°C)	TCO thin film materials
1.1×10^{-3} Ω cm	200	~94	RF magnetron sputtering	10	78.0	AZO thin films[62]
2.14×10^{-4} Ω cm	RT	~90	PLD	10	75.0	GZO thin films[63]
1.30×10^{-4} Ω cm	500	~90	RF magnetron sputtering	42	90.0	GZO thin films[36]
72.51 Ω. sq^{-1} (sheet resistance)	RT	~80.8	RF magnetron sputtering	12	44.4	AZO thin films[64]
65.71 Ω. sq^{-1} (sheet resistance)	RT	79.7	Metal organic CVD	12	45.3	FTO thin films[64]
43.96 Ω. sq^{-1} (sheet resistance)	RT	82.1	Metal organic CVD	12	48.9	AZO/FTO double layer thin films[64]
36.7 Ω. sq^{-1} (sheet resistance)	RT	82.1	Metal organic CVD	12	71.8	FTO/AZO double layer thin films[64]
10.1×10^{-3} Ω cm	**350**	**~81**	**PLD**	**10**	**76.0**	**GZO thin films (this work)**

tin oxide), and FTO/AZO double layer thin film materials for TFTHs applications in Table II.

CONCLUSION

In conclusion, we were able to optimize and study a highly transparent and conductive GZO thin film deposited on glass substrates by varying the oxygen partial pressure from 0 to 10 mTorr using PLD. The as-grown GZO films without oxygen displayed an excellent electrical resistance as low as ~5 Ω while remaining above 85% transparent in the visible wavelength region. The XPS study revealed that increasing oxygen partial pressure favors the reduction in oxygen vacancies, which is normally seen in GZO samples grown in a high vacuum environment. The GZO thin films demonstrate excellent electro-thermal properties via the joule heating effect when deposited under an oxygen partial pressure of 10 mTorr. The 10 mTorr GZO thin film produced higher temperatures close to 75 °C with an applied voltage of ≤10 V. These results can be used in various thin-film heating applications, such as automobile defrosters, airplane de-icing, and energy-efficient, low-powered smart windows.

ACKNOWLEDGMENTS

This work was supported by the NSF-CREST (CREAM) under Grant No. HRD 1547771.

AUTHOR DECLARATIONS

Conflict of Interest

The authors have no conflicts to disclose.

Author Contributions

Jasmine Beckford: Conceptualization (equal); Writing – original draft (equal). **Makhes K Behera**: Conceptualization (equal); Writing – original draft (equal). **Kelsea Yarbrough**: Validation (equal); Visualization (equal); Writing – review & editing (equal). **Sangram K Pradhan**: Conceptualization (equal); Data curation (equal); Supervision (equal); Validation (equal); Visualization (equal); Writing – original draft (equal); Writing – review & editing (equal). **Messaoud Bahoura**: Conceptualization (equal); Funding acquisition (equal); Project administration (equal); Supervision (equal); Validation (equal); Visualization (equal); Writing – review & editing (equal).

DATA AVAILABILITY

The data that support the findings of this study are available from the corresponding author upon reasonable request.

REFERENCES

[1] R. Zhou *et al.*, "Stretchable heaters with composites of an intrinsically conductive polymer, reduced graphene oxide and an elastomer for wearable thermotherapy," J. Mater. Chem. C **5**(6), 1544–1551 (2017).
[2] W. Lan *et al.*, "Ultraflexible transparent film heater made of Ag nanowire/PVA composite for rapid-response thermotherapy pads," ACS Appl. Mater. Interfaces **9**, 6644–6651 (2017).
[3] M. Katayama, "TFT-LCD technology," Thin Solid Films **341**, 140–147 (1999).
[4] M. Gaillet, L. Yan, and E. Teboul, "Optical characterizations of complete TFT–LCD display devices by phase modulated spectroscopic ellipsometry," Thin Solid Films **516**, 170–174 (2007).
[5] S. Ameen *et al.*, "An insight into atmospheric plasma jet modified ZnO quantum dots thin film for flexible perovskite solar cell: Optoelectronic transient and charge trapping studies," J. Phys. Chem. C **119**, 10379–10390 (2015).
[6] M. Dosmailov *et al.*, "Transparent conductive ZnO layers on polymer substrates: Thin film deposition and application in organic solar cells," Thin Solid Films **591**, 97–104 (2015).
[7] S. Fernández *et al.*, "Effect of argon plasma-treated polyethylene terepthalate on ZnO: Al properties for flexible thin film silicon solar cells applications," Sol. Energy Mater. Sol. Cells **133**, 170–179 (2015).

[8]Z.-F. Shi *et al.*, "Epitaxial growth of vertically aligned ZnO nanowires for bidirectional direct-current driven light-emitting diodes applications," CrystEngComm **17**, 40–49 (2015).
[9]H.-J. Seok, J.-K. Kim, and H.-K. Kim, "Effective passivation of Ag nanowire network by transparent tetrahedral amorphous carbon film for flexible and transparent thin film heaters," Sci. Rep. **8**, 13521 (2018).
[10]S. Hong *et al.*, "Highly stretchable and transparent metal nanowire heater for wearable electronics applications," Adv. Mater. **27**, 4744–4751 (2015).
[11]H.-Y. Lu *et al.*, "Highly transparent and flexible polyimide–AgNW hybrid electrodes with excellent thermal stability for electrochromic applications and defogging devices," J. Mater. Chem. C **3**, 3629–3635 (2015).
[12]S. Choi *et al.*, "Stretchable heater using ligand-exchanged silver nanowire nanocomposite for wearable articular thermotherapy," ACS Nano **9**, 6626–6633 (2015).
[13]Z. Xian *et al.*, "A practical ITO replacement strategy: Sputtering-free processing of a metallic nanonetwork," Adv. Mater. Technol. **2**, 1700061 (2017).
[14]H. H. Khaligh *et al.*, "Silver nanowire transparent electrodes for liquid crystal-based smart windows," Sol. Energy Mater. Sol. Cells **132**, 337–341 (2015).
[15]B. Han *et al.*, "Uniform self-forming metallic network as a high-performance transparent conductive electrode," Adv. Mater. **26**, 873–877 (2014).
[16]H.-G. Cheong *et al.*, "Silver nanowire network transparent electrodes with highly enhanced flexibility by welding for application in flexible organic light-emitting diodes," ACS Appl. Mater. Interfaces **6**, 7846–7855 (2014).
[17]T. Sannicolo *et al.*, "Metallic nanowire-based transparent electrodes for next generation flexible devices: A review," Small **12**, 6052–6075 (2016).
[18]C.-C. Lin, D.-X. Lin, and S.-H. Lin, "Degradation problem in silver nanowire transparent electrodes caused by ultraviolet exposure," Nanotechnology **31**, 215705 (2020).
[19]G.-S. Liu *et al.*, "Comprehensive stability improvement of silver nanowire networks via self-assembled mercapto inhibitors," ACS Appl. Mater. Interfaces **10**, 37699–37708 (2018).
[20]A. Madeira *et al.*, "Increasing silver nanowire network stability through small molecule passivation," Nanomaterials **9**, 899 (2019).
[21]H. G. Manning *et al.*, "The electro-optical performance of silver nanowire networks," Sci. Rep. **9**, 11550 (2019).
[22]C. Liu *et al.*, "Fatigue and the electrical resistance of silver nanowire networks," Scr. Mater. **181**, 97–100 (2020).
[23]K.-W. Seo *et al.*, "Simple brush painted Ag nanowire network on graphene sheets for flexible organic solar cells," J. Vac. Sci. Technol., A **32**, 061201 (2014).
[24]Y. U. Jung *et al.*, "Electromechanical properties of graphene transparent conducting films for flexible electronics," Curr. Appl. Phys. **13**, 1331–1334 (2013).
[25]L. Gan *et al.*, "Connection-improved conductive network of carbon nanotubes in a rubber cross-link network," ACS Appl. Mater. Interfaces **10**, 18213–18219 (2018).
[26]J. Che, T. Çagin, and W. A. Goddard III, "Thermal conductivity of carbon nanotubes," Nanotechnology **11**, 65 (2000).
[27]B. Kumanek and D. Janas, "Thermal conductivity of carbon nanotube networks: A review," J. Mater. Sci. **54**, 7397–7427 (2019).
[28]J. A. Isaacs *et al.*, "Economic assessment of single-walled carbon nanotube processes," J. Nanopart. Res. **12**, 551–562 (2010).
[29]R. H. Baughman, A. A. Zakhidov, and W. A. De Heer, "Carbon nanotubes–the route toward applications," Science **297**, 787–792 (2002).
[30]W. M. Cranton *et al.*, "Enhanced electrical and optical properties of room temperature deposited Aluminium doped Zinc Oxide (AZO) thin films by excimer laser annealing," Opt. Lasers Eng. **80**, 45–51 (2016).
[31]J. Beckford *et al.*, "Gallium doped zinc oxide thin films as transparent conducting oxide for thin-film heaters," AIP Adv. **11**, 075208 (2021).
[32]G. Jo and J.-H. Koh, "Laser annealing effects on Ga dopants for ZnO thin films for transparent conducting oxide applications," Ceram. Int. **45**, 6190–6197 (2019).
[33]R. N. Chauhan *et al.*, "Development of Al-doped ZnO thin film as a transparent cathode and anode for application in transparent organic light-emitting diodes," RSC Adv. **6**, 86770–86781 (2016).
[34]A. Varanytsia, L. Weng, T.-C. Lin, J. Yang, and L.-C. Chien, "High-performance and low-cost aluminum zinc oxide and gallium zinc oxide electrodes for liquid crystal displays," J. Display Technol. **12**, 1033–1039 (2016).
[35]H. Kim, A. Piqué, J. S. Horwitz, H. Murata, Z. H. Kafafi, C. M. Gilmore, D. B. Chrisey *et al.*, "Effect of aluminum doping on zinc oxide thin films grown by pulsed laser deposition for organic light-emitting devices," Thin Solid Films **377-378**, 798–802 (2000).
[36]J. H. Kim, B. D. Ahn, C. H. Kim, K. A. Jeon, H. S. Kang, and S. Y. Lee, "Heat generation properties of Ga doped ZnO thin films prepared by RF-magnetron sputtering for transparent heaters," Thin Solid Films **516**, 1330–1333 (2008).
[37]T. Yamada *et al.*, "Effects of oxygen partial pressure on doping properties of Ga-doped ZnO films prepared by ion-plating with traveling substrate," Surf. Coat. Technol. **201**, 4004–4007 (2006).
[38]A. Shyichuk and E. Zych, "Oxygen vacancy, oxygen vacancy–vacancy pairs, and Frenkel defects in cubic lutetium oxide," J. Phys. Chem. C **124**, 14945–14962 (2020).
[39]F. Gunkel *et al.*, "Oxygen vacancies: The (in) visible friend of oxide electronics," Appl. Phys. Lett. **116**, 120505 (2020).
[40]X. Li *et al.*, "Effect of oxygen pressure on GZO film as active layer of the TFT fabricated at room temperature," Superlattices Microstruct. **137**, 106317 (2020).
[41]Y. Liu *et al.*, "Improved performance of transparent conductive Cu-based GZO multilayer thin films on flexible substrates via two Al_2O_3 layers and oxygen-containing atmosphere," J. Alloys Compd. **874**, 159949 (2021).
[42]P. Mondal *et al.*, "Effect of oxygen partial pressure on the behavior of Ga-doped ZnO/p-Si heterojunction diodes fabricated by reactive sputtering," J. Mater. Sci.: Mater. Electron. **32**, 4248–4257 (2021).
[43]A. P. Chen *et al.*, "Strong oxygen pressure dependence of ferroelectricity in $BaTiO_3/SrRuO_3/SrTiO_3$ epitaxial heterostructures," J. Appl. Phys. **114**, 124101 (2013).
[44]Z. Harrell *et al.*, "Oxygen content tailored magnetic and electronic properties in cobaltite double perovskite thin films," Appl. Phys. Lett. **110**, 093102 (2017).
[45]W. C. Yang *et al.*, "Epitaxial thin films of pyrochlore iridate $Bi_{2+x}Ir_{2-y}O_{7-\delta}$: Structure, defects and transport properties," Sci. Rep. **7**, 7740 (2017).
[46]D. Girbovan , "Structure, morphology and optical properties of Al-doped ZnO thin films," Stud. Univ. Babes-Bolyai Chem. **56**, 213 (2011).
[47]J. J. Ding *et al.*, "Influence of Al-doping on the structure and optical properties of ZnO films," Physica B **404**, 2439–2443 (2009).
[48]D. Koretomo, S. Hamada, Y. Magari, and M. Furuta, "Quantum confinement effect in amorphous In–Ga–Zn–O heterojunction channels for thin-film transistors," Materials **13**, 1935 (2020).
[49]K. M. Sandeep *et al.*, "Influence of Ga doping ratio on the saturable absorption mechanism in Ga doped ZnO thin solid films processed by sol–gel spin coating technique," J. Phys. D: Appl. Phys. **50**, 095105 (2017).
[50]H.-K. Kim *et al.*, "Dependence of electrical, optical, and structural properties on the thickness of GZO films prepared by CRMS," J. Electrochem. Soc. **159**, H38 (2011).
[51]H. Yoon *et al.*, "Effects of Ga concentration on the structural, electrical and optical properties of Ga-doped ZnO thin films grown by sol-gel method," J. Korean Phys. Soc. **64**, 109–113 (2014).
[52]Z. Z. You and G. J. Hua, "Electrical, optical and microstructural properties of transparent conducting GZO thin films deposited by magnetron sputtering," J. Alloys Compd. **530**, 11–17 (2012).
[53]Q. Q. Mohammed *et al.*, "Oxygen pressure effects on optical properties of ZnO prepared by reactive pulsed laser deposition," AIP Conf. Proc. **2213**(1), 020237 (2020).
[54]K.-G. Zheng, T.-Y. Yang, and Z. Guo, "Porous Pb-doped ZnO nanobelts with enriched oxygen vacancies: Preparation and their chemiresistive sensing performance," Chemosensors **10**, 96 (2022).
[55]W. Yan *et al.*, "MOF-derived porous hollow Co_3O_4@ ZnO cages for high-performance MEMS trimethylamine sensors," ACS Sensors **6**, 2613–2621 (2021).
[56]S. Kim *et al.*, "Influence of substrate temperature and oxygen/argon flow ratio on the electrical and optical properties of Ga-doped ZnO thin films prepared by rf magnetron sputtering," Cryst. Res. Technol. **41**, 1194–1197 (2006).
[57]M. K. Roul, B. Obasogie, G. Kogo, J. R. Skuza, R. M. Mundle, and A. K. Pradhan, "Transparent and flexible heaters based on Al:ZnO degenerate semiconductor," J. Appl. Phys. **122**, 135110 (2017).

[58]N. F. Mott and L. Friedman, *Metal-insulator Transition* (Taylor & Francis, London, 1974), p. XVI.
[59]R. C. Budhani *et al.*, "Magneto-transport in epitaxial films of the degenerate semiconductor $Zn_{1-x}Co_xO$," J. Phys.: Condens. Matter **17**, 75 (2005).
[60]J. Han, P. Q. Mantas, and A. M. R. Senos, "Effect of Al and Mn doping on the electrical conductivity of ZnO," J. Eur. Ceram. Soc. **21**, 1883 (2001).
[61]M. N. Alexander and D. F. Holcomb, "Semiconductor -to-metal transition in n-type group IV semiconductor," Rev. Mod. Phys. **40**, 815 (1968).
[62]Y. Furubayashi *et al.*, "A transparent metal: Nb-doped anatase TiO_2," Appl. Phys. Lett. **86**, 252101 (2005).
[63]B. D. Ahn, S. H. Oh, D. U. Hong, D. H. Shin, A. Moujoud, and H. J. Kim, "Transparent Ga-doped zinc oxide-based window heaters fabricated by pulsed laser deposition," J. Cryst. Growth **310**, 3303–3307 (2008).
[64]A. Y. Kim, K. Lee, J. H. Park, D. Byun, and J. K. Lee, "Double-layer effect on electrothermal properties of transparent heaters," Phys. Status Solidi A **211**, 1923–1927 (2014).